Check for updates

Single-molecule conductance of double-stranded RNA oligonucleotides†

Subrata Chandra, Keshani G. Gunasinghe Pattiya Arachchillage, Evgenii Kliuchnikov, Farkhad Maksudov, Steven Ayoub, Valeri Barsegov and Juan M. Artés Vivancos [ID] *

RNA oligonucleotides are crucial for a range of biological functions and in many biotechnological applications. Herein, we measured, for the first time, the conductance of individual double-stranded (ds)RNA molecules and compared it with the conductance of single DNA : RNA hybrids. The average conductance values are similar for both biomolecules, but the distribution of conductance values shows an order of magnitude higher variability for dsRNA, indicating higher molecular flexibility of dsRNA.

Department of Chemistry, University of Massachusetts, Lowell, 01854 MA, USA.
E-mail: juan_artesvivancos@uml.edu; Tel: (+1)9789344337
†Electronic supplementary information (ESI) available. See DOI: 10.1039/d1nr06925j

Juan M. Artés Vivancos is an assistant professor in the Department of Chemistry at the University of Massachusetts Lowell. After obtaining a Ph.D. from the University of Barcelona working in single molecule bioelectronics, he was a postdoctoral associate at the ECE Department of the University of California, Davis, developing new electrical methods for detecting oligonucleotides. He was awarded an individual

Juan M. Artés Vivancos

Marie Skłodowska-Curie and a Human Frontiers postdoctoral fellowship to learn physicochemical optical techniques and nonlinear ultrafast spectroscopies to study biological processes. His research interests span from single-molecule biophysics and electrical nanobiosensors to developing new microscopy and spectroscopy techniques that provide high spatiotemporal resolution. When he is not having fun in the lab, he also enjoys reading sci-fi, playing guitar, and capoeira.

Microsecond Molecular Dynamics simulations explain this difference and provide structural insights into the higher stability of DNA : RNA duplex with atomic level of detail. The rotations of 2'-OH groups of the ribose rings and the bases in RNA strands destabilize the duplex structure by weakening base stacking interactions, affecting charge transport, and making single-molecule conductance of dsRNA more variable (dynamic disorder). The results demonstrate that a powerful combination of state-of-the-art biomolecular electronics techniques and computational approaches can provide valuable insights into biomolecules' biophysics with unprecedented spatial resolution.

Oligonucleotides play essential roles in cell functions[1,2] and several biotechnological applications.[3,4] In particular, RNA has recently gained importance in the research focus for several reasons. Not only do several pathogens (*e.g.*, SARS-CoV2) have RNA genomes, but many therapeutic, biotechnological, and modern molecular technologies (*e.g.*, gene editing[5]) also use RNA and its biophysics. Additionally, nucleic acids have interesting electronic and self-assembly properties that make them promising candidates as building blocks for nanotechnological[6,7] and sensory applications.[8,9] For these reasons, it is crucial to characterize the biophysical properties of RNA, particularly at the single-molecule level.

In the last decades, single-molecule techniques have allowed biological and biophysical studies with unprecedented resolution.[10–12] On the biomolecular electronics side, the electronic and charge-transport (CT) properties of short oligonucleotides have been reported.[13,14] They have resulted in proposing proof-of-concept sensors based on individual biomolecule detection.[8]

Short double-stranded (ds)DNA and DNA : RNA hybrids have been extensively characterized, including the length,[13–15] sequence,[13–16] and conformational dependence[17] of the conductance of individual molecules. Although some controversy remains regarding the role of the nucleic acid backbone in mediating the CT,[18] there is a consensus that the CT process is mainly mediated by base stacking in the double helix and

deeply affected by the delocalization length through the bases.[14,17,19] Consequently, changes in conformation[17] or base mismatches that disrupt the base stacking pattern; or the delocalization length[8,16] can modify the conductance value measured in experiments. Also, despite its biophysical and biological importance, the single-molecule electronic properties of dsRNA have not yet been reported.

Here, we use a combination of single-molecule conductance experiments and computer simulations to explore the conductance of individual dsRNA molecules. The conductance histograms show that dsRNA has a conductance within experimental error of DNA:RNA hybrids of the same nucleotide sequence, in agreement with the notion that both biomolecules are in the A-form.[15,17] However, our results show differences in the distribution of molecular conductance values for dsRNA *vs.* DNA:RNA. The electrical conductance histogram for dsRNA is an order of magnitude broader than the histogram for DNA:RNA, suggesting higher molecular flexibility and lower stability for dsRNA. To help provide dynamic structural insights into the biophysics of these molecules, we employed Molecular Dynamics (MD) simulations of dsRNA and DNA:RNA duplexes, which show that conformational transitions in the ribose rings and bases in RNA strands destabilize base stacking, affecting the CT process.

We used the Scanning Tunneling Microscope-assisted Break Junction (STM-BJ)[20] method to measure individual biomolecule conductance (see the ESI† for detailed materials and methods). Briefly, the electrodes of a Scanning Tunneling Microscope (STM) are repeatedly brought into contact and retracted in the presence of a buffer solution containing the oligonucleotides modified with thiol binding groups at 5′ and 3′ ends so that they can bind to the electrodes (Fig. 1a). At the same time, the current (I) in the molecular junction is measured by applying a moderate bias voltage (V). The molecular conductance (G) can be obtained from $G = I/V$ by recording thousands of conductance *vs.* distance traces and combining them into conductance histograms (using an automatic selection algorithm[21]). After saving 5000–1000 traces per experiment, selectivity (defined as the number of curves containing significant "steps") ranged from less than 1% in blank and control experiments to 5 to 10% in experiments with nucleic acids. This assists in obtaining the most probable molecular conductance and in accessing subpopulations of molecular conformations.[17,22] These characteristics provide valuable information about the biophysical properties of oligonucleotide molecules[12,17] and the molecular-electrode contacts they form.[22,23] These experiments were performed by applying a 100 mV bias voltage between the tip and the substrate in a phosphate buffer media. For this reason, it is necessary to cover the STM tips with Apiezon wax to isolate them from any leakage currents.

Fig. 1a shows an idealized schematic of the experimental setup for the 11 base pairs (bp) DNA:RNA hybrid oligonucleotide bridging between two gold electrodes. Fig. 1b shows raw data of conductance-distance measurements for dsRNA (blue traces), DNA:RNA hybrids (red curves), and
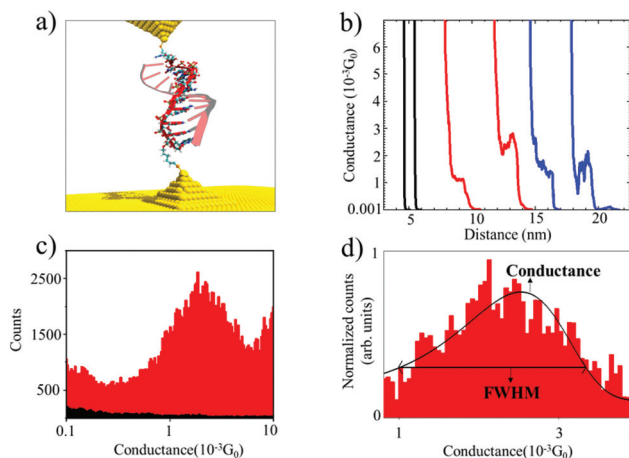

Fig. 1 (a) Schematic illustration of the experimental setup, showing an oligonucleotide attached to two Au electrodes (solid strand: RNA probe, semi-transparent strand: target RNA or target DNA). (b) Raw conductance *vs.* distance curves (black for phosphate buffer blank, red for DNA:RNA duplex, and blue for dsRNA). (c) Conductance histogram for DNA:RNA hybrid (red) showing the most probable conductance value (*i.e.*, conductance peak at $1.7 \times 10^{-3} G_0$). The background signals from a control buffer experiment are shown in black. Experiments were performed with a 100 mV applied bias voltage. (d) Normalized Gaussian distribution of the conductance values for DNA:RNA hybrids showing standard deviations estimated as the full width at half maximum (FWHM).

control measurements (clean Au substrate in phosphate buffer, in black); see ESI Fig. S1–S3† for more results from control experiments. The blank phosphate buffer shows no detectable conductance events or "steps", whereas dsRNA and DNA:RNA duplexes show similar features in the $0.001G_0$ range (G_0 is $2e^2/h$, where e is the electron charge and h is the Planck constant), indicating the formation of biomolecular junctions. By analyzing thousands of individual conductance-distance curves, we obtained the histogram-based estimates of the conductance distributions. These can be used to calculate the most probable conductance (peak conductance) and conductance variability quantified by the full width at half maximum (FWHM). Fig. 1c and d show the conductance histograms for an 11 bp DNA:RNA hybrid (CCCGCGCGCCC) constructed with raw data with and without baseline subtraction and normalization (to the highest number of counts in the histogram), respectively. Fig. 1d also includes a Gaussian curve fit centered at $1.7 \times 10^{-3} G_0$, in agreement with previously reported values for this DNA:RNA hybrid[15] and other A-form oligonucleotides.[17] This single-molecule conductance value is remarkably high for a biomolecule around 2.5 nm long, but not surprising considering this is an A-form GC-rich oligonucleotide sustaining a hopping charge transport process with a high coherence length.[15,17]

The results of conductance measurements for an 11 bp dsRNA and DNA:RNA hybrid with the same sequence (CCCGCGCGCCC) are compared in Fig. 2, which shows the normalized conductance histograms (Fig. 2a), as well as conductance statistics (Fig. 2b) from the Gaussian curve fitting,
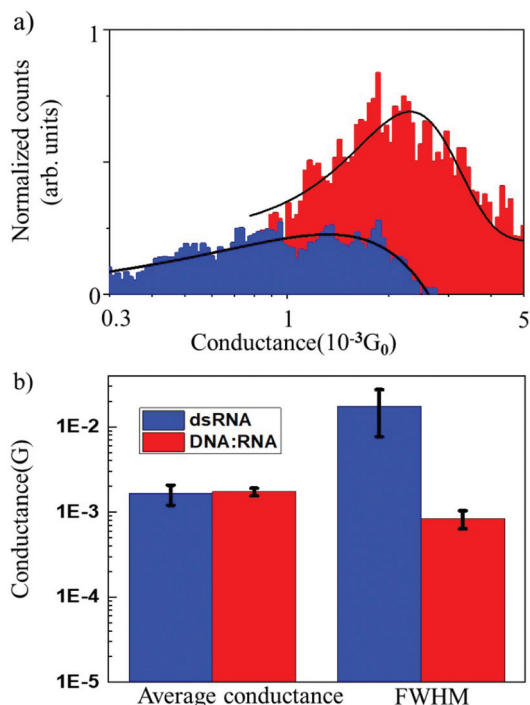
Fig. 2 (a) Comparison of the normalized conductance histograms for dsRNA (blue) and DNA : RNA (red). (b) Average conductance values and FWHM, their standard deviations for dsRNA duplexes and DNA : RNA hybrids. All the experiments were done with a 100 mV applied bias voltage.

i.e., the most probable conductance and standard deviations estimated as the FWHM.

The single-molecule conductance for dsRNA is $1.6 \times 10^{-3} G_0$ *vs.* $1.7 \times 10^{-3} G_0$ for DNA : RNA, without statistically significant differences. This is not surprising since dsRNA is an A-form oligonucleotide with a similar structure to DNA : RNA and is consistent with the notion that the conformation of the oligonucleotide plays a crucial role in defining the electronic and CT properties.[17] However, the distribution of conductance values is broader for dsRNA than for DNA : RNA by one order of magnitude (Fig. 2a; see also Table 1). Higher standard deviations for dsRNA indicate a larger dispersion in the molecular conductance values for dsRNA. Since single-molecule conductance is mainly influenced by the base stacking, which depends on the oligonucleotides' molecular conformation, these results point to a more considerable extent of conformational fluctuations for dsRNA (larger dynamic disorder) and increased molecular flexibility. This is remarkable because a

Table 1 Statistics of single-molecule conductance for dsRNA and DNA : RNA hybrids: average and standard deviations for conductance and FWHM values

| Molecule	Average conductance ($\times 10^{-3} G_0$)	FWHM ($\times 10^{-2} G_0$)
dsRNA	1.63 ± 0.43	1.75 ± 0.98
DNA : RNA hybrid	1.72 ± 0.18	0.083 ± 0.02

subtle difference in the oligonucleotide composition (RNA *vs.* DNA) translates into a noticeable change in measured single-molecule conductance. Notably, the results obtained demonstrate that STM-BJ is a sensitive technique capable of detecting small changes in the conformation-dependent biophysical properties of individual biomolecules.[12]

To provide a structure-based interpretation for the single biomolecular conductance experiments, we turned to computational molecular modeling. Molecular Dynamics (MD) simulations play an increasingly important role not only in complementing experimental techniques but also in helping to understand the physical properties of single biomolecules at an atomic level of detail.[24–28] Here, we employed MD simulations, accelerated on Graphics Processing Units (GPUs),[29] to explore and directly compare the conformational dynamics of dsRNA *vs.* DNA : RNA hybrids in a long timescale spanning a few microseconds to explain the difference in their electrical conductance characteristics.

Molecular modeling of dsRNA and DNA : RNA hybrids, including the sequence reconstruction, MD simulation protocol, and analyses of the output from MD simulations, are described in detail in ESI.† Briefly, SimRNA software[30] was utilized to model RNA and DNA sequences. The MD simulations for dsRNA and DNA : RNA were performed for 1 μs using the CUDA version of pmemd[31] and GPU accelerated version[32] of AMBER 20 software package.[33] The force fields bsc0$_{\chi OL3}$[34] and bsc0[35] used for RNA and DNA strands are a part of ff14SB.[36] The TIP3P model was used to describe water molecules explicitly.[37] A total of 3730 water molecules were included in the solvation box with volume 143.4 Å. The phosphate groups in the backbone of RNA and DNA strands were neutralized using 20 Na$^+$ ions, and excess ions (0.1 M) were added to mimic the experimental conditions (9 Na$^+$ ions and 9 Cl$^-$ ions). We carried out two independent sets of MD simulations of dsRNA and DNA : RNA molecules. In the first set, the ends of the molecules were not constrained. To mimic the effect of experimental constraints on the molecular flexibility of dsRNA and DNA : RNA hybrid due to coupling to junctions, in the second set, we "clamped" (harmonically constrained) the 5′-end and the 3′-end phosphorus atoms in dsDNA and DNA : RNA molecules. The two strands forming the dsRNA and DNA : RNA duplexes were found to be stable during 1 μs MD simulations.

First, we compared the conformational variability in dsRNA *vs.* DNA : RNA structures (see S4 and S5†). Fig. 3 shows both structures undergoing large-amplitude conformational fluctuations while preserving the duplex arrangement of RNA and DNA helical structure. Because the intra-strand interactions (base stacking) and inter-strand interactions (base pairing) are known to reinforce the duplex structure of RNA and DNA molecules, we, first, qualitatively described the strength of base stacking and base pairing in dsRNA and DNA : RNA hybrid (see ESI†). We found that the most robust base stacking bonds, *i.e.*, the most persistent (longer-lasting) base stacks, form in DNA and RNA strands in the center of dsRNA and DNA : RNA molecules (Fig. 3b). The weakest (or short-lasting) base stacking bonds are formed at the 3′- and 5′-ends (Fig. 3b).
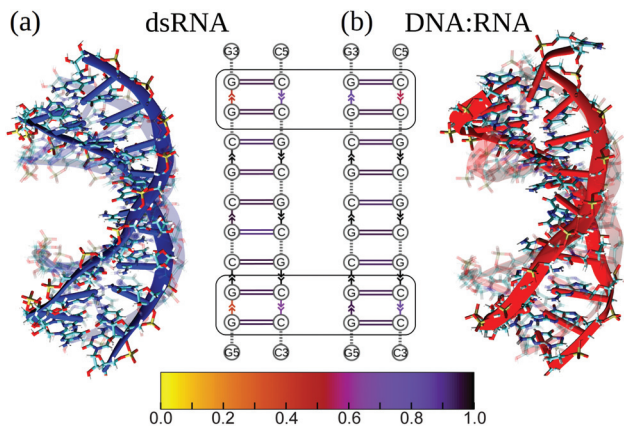
Fig. 3 Atomic structures and maps of intra-strand (base stacking) and inter-strand (base pairing) interactions in dsRNA (in blue; panel a) and DNA : RNA (in red; panel b). Transient structures are superimposed with the average structures (displayed in the background), showing the secondary structure (blue and red ribbons) and chemical bonds. In interaction maps, vertical arrows and horizontal lines denote base stacking and base pairing arrangements. The color code reflects the strength of base stacking bonds; the darker (lighter) color, the more (less) persistent or stronger (weaker) the bond is. Bounded regions show the weakest base stacking bonds at the 5′- and 3′-ends in dsRNA and DNA : RNA duplexes.

This agrees well with the results of previous experimental studies on other sequences.[38]

Next, we compared conformational fluctuations in dsRNA and DNA : RNA by analyzing the root-mean-square deviations (RMSD) and end-to-end distance X. These metrics of molecular flexibility can be accessed using the simulation output (see ESI†). The RMSD was calculated for the backbone heavy atoms of the RNA or DNA strands. The end-to-end distance X was calculated as the distance between the first (at the 5′-end) and the last (at the 3′-end) P-atoms in the complementary strand in dsRNA or DNA strand in DNA : RNA (ESI†). The time-dependent profiles of RMSD and X are compared in Fig. 4a. The RMSD profile for dsRNA lies above the RMSD profile for DNA : RNA by ≈1 Å, which shows that dsRNA is characterized by a more considerable molecular flexibility than DNA : RNA. Interestingly, the profile of X for dsRNA is lower than that for DNA : RNA by ≈0.5 nm, which means that dsRNA is on average a shorter duplex than DNA : RNA. We also analyzed the statistics of RMSDs and X (averages and standard deviations; see Table 2). The average RMSDs with standard deviations comes to 2.0 ± 0.2 Å for dsRNA *vs.* 1.2 ± 0.1 Å for DNA : RNA. The average X is 2.9 ± 0.1 nm for dsRNA *vs.* 3.3 ± 0.1 nm for DNA : RNA (Table 2). The statistics of RMSD and X did not change upon constraining the 5′-end and the 3′-end phosphorus atoms in dsRNA and DNA : RNA. Therefore, these numbers show that our conclusions about the differences in molecular flexibility for dsRNA *vs.* DNA : RNA are statistically significant.

The results of MD simulations demonstrate a larger extent of conformational fluctuations in dsRNA compared to
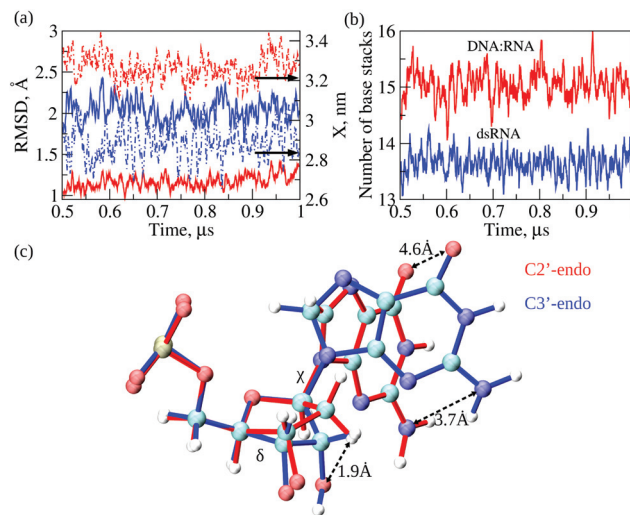
Fig. 4 Dynamic properties of the dsRNA *vs.* DNA : RNA duplex: RMSD of atomic positions (left *y*-axis) and end-to-end distance X (right *y*-axis) displayed in panel a; number of base stacking interactions stabilizing the duplex structure (panel b), and relative orientations of nucleotide bases in RNA strand with C3′-*endo* ribose and in DNA strands with C2′-*endo* ribose (panel c). The C-, N-, O- and H-atoms are represented by blue, cyan, red, and gray balls, respectively. Also displayed in panel *c* are the dihedral angles δ and χ, which quantify, respectively, the rotations of ribose rings and bases resulting in 3.7 Å and 4.6 Å shift in the positions of NH_2- and CO-groups.

Table 2 Comparison of dynamic structural properties and excluded volume interactions in dsRNA *vs.* DNA : RNA. Shown are the root-mean-square deviations (RMSD) of atomic positions, end-to-end distance (X), number of base pairs (N_{bp}) and base stacks (N_{bs}), dihedral angles δ and χ, and van der Waals energy E_{vdW}

Molecule	dsRNA	DNA : RNA hybrid
RMSD, Å	2.0 ± 0.2	1.2 ± 0.1
X, nm	2.9 ± 0.1	3.3 ± 0.1
N_{bp}	11.3 ± 0.3	10.7 ± 0.8
N_{bs}	13.6 ± 0.6	15.0 ± 0.8
δ, deg	78 ± 7	116 ± 23
χ, deg	197 ± 8	236 ± 24
E_{vdW}, kcal mol^{-1}	−179 ± 4	−162 ± 4

DNA : RNA. These findings correlate well with more significant standard deviations observed for the experimental values of molecular conductance (see Table 1 and Fig. 2b). Because the base-stacking interactions influence the conductance of oligonucleotides, we next analyzed the dynamics of base-stacking interactions in dsRNA and DNA : RNA hybrids. The time profiles of the number of base-stacking bonds are compared for dsRNA and DNA : RNA in Fig. 4b, which shows that fewer base-stacking bonds reinforce the duplex structure in dsRNA duplex than in DNA : RNA duplex. The average number of base stacks N_{bs} comes to 13.6 ± 0.6 for dsRNA *vs.* 15.0 ± 0.8 for DNA : RNA (Table 2). Interestingly, the average number of base pairs N_{bp} is 11.3 ± 0.3 for dsRNA *vs.* 10.7 ± 0.8 for DNA : RNA (Table 2), which are not statistically different. These results show that

the weaker base-stacking bonds do not imply the weaker base-pairing bonds in the dsRNA duplex. The statistics of N_{bp} and N_{bs} did not change upon constraining the 5′-end and 3′-end of dsRNA and DNA : RNA duplexes.

That shorter dsRNA is more flexible and has fewer base-stacking bonds than DNA : RNA hybrids prompted us to explore the structural origin underlying these differences. We carried out a detailed analysis of transient structures of dsRNA and DNA : RNA as observed in the course of 1 μs MD simulations. We analyzed and compared the statistics of dihedral angles, namely the torsion angle δ formed by a quartet of heavy atoms C5′–C4′–C3′–O3′ and the glycosidic angle χ formed by heavy atoms O4′–C1′–N9–C4 in purine bases and atoms O4′–C1′–N1–C2 in pyrimidine bases (see Fig. 4c). The torsion angle δ quantifies rotation of the ribose ring with respect to the backbone, whereas glycosidic angle χ quantifies rotation of the base with respect to the ribose ring (Fig. 4c). The statistics of δ and χ are compared for dsRNA vs. DNA : RNA in Table 2, which shows large statistically significant differences: δ is 116 ± 23° for DNA : RNA vs. 78 ± 7° for dsRNA; and χ is 236 ± 24° for DNA : RNA vs. 197 ± 8° for dsRNA. The statistics of dihedral angles δ and χ did not change upon constraining the 5′- and 3′-ends of dsRNA and DNA : RNA duplexes.

Structural analysis of RNA and DNA strands in dsRNA and DNA : RNA hybrid revealed essential differences in the packing of nucleobases in dsRNA vs. DNA : RNA duplexes. Due to the C3′-endo arrangement of ribose rings in the RNA strand; the ribose ring is rotated $\Delta\delta \approx 116{-}78 = 38°$ with respect to the phosphate backbone as compared to C2′-endo arrangement of ribose ring in the DNA strand, and the base is rotated $\Delta\chi \approx 236{-}197 = 39°$ with respect to the ribose ring (Fig. 4c). These rotations result in the 1.9 Å shift in the C3′-atom position, 3.7 Å shift in the position of NH_2-group, and 4.6 Å shift in the position of CO-group (Fig. 4c). We hypothesize that a driving force for these large-amplitude structural rearrangements is the propensity of dsRNA to minimize steric clashes in RNA strands. Therefore, we calculated the values of van der Waals energy E_{vdW}, which quantifies the excluded volume interactions, for an RNA strand in the dsRNA duplex and in DNA : RNA duplex (ESI†). The more negative value of E_{vdW} implies smaller steric clashes and weaker excluded volume interactions. E_{vdW} came to −179 ± 4 kcal mol^{-1} for dsRNA vs. −162 ± 4 kcal mol^{-1} for DNA : RNA hybrid (see Table 2). Hence, the structural rearrangements in dsRNA, i.e., rotations of ribose rings and bases described above result in lowering the energy associated with excluded volume interactions in dsRNA duplex by $\Delta E_{vdW} = 179{-}162 = 17$ kcal mol^{-1}. This conclusion did not change when we analyzed the results of MD simulations for dsRNA and DNA : RNA with constrained ends. This agrees with the notion that the presence of OH-groups in RNA results in lower chemical stability of RNA compared to DNA, thus, making DNA more tailored for the long-term storage of genetic information[39] and making RNA more capable of carrying out various regulatory functions.[40]

In summary, for the first time, we explored the single-molecule electrical conductance of dsRNA and compared the dsRNA conductance with that for DNA : RNA hybrids formed by identical sequences. The average conductance values were similar for both biomolecules, but the dsRNA conductance was more variable. The conductance distribution for dsRNA is one order of magnitude broader than that for DNA : RNA hybrids, which indicates that dsRNA is a more flexible duplex. We employed computational molecular modeling to uncover the structural underpinnings of the experimental results. The MD simulations of dsRNA and DNA : RNA both without and with constrained ends confirmed higher flexibility of dsRNA and illuminated, in atomic detail, the molecular mechanism of this effect. The results obtained demonstrate that the CT process in oligonucleotides is mainly mediated by base stacking. Our experiments also show that single-molecule conductance is a sensitive parameter and that STM-BJ is a powerful method capable of detecting even slight differences in the dynamic structural properties of biomolecules. Our results are a good starting point to motivate future biophysical characterization of single biomolecules of larger complexity.

Author contributions

JMAV and SC conceptualized and designed the research. SC, KGGPA, SA, and JMAV performed experimental work and data analyses. EK, FM, and VB carried out the computational work and data analyses. All the authors discussed the results and contributed to manuscript writing.

Conflicts of interest

There are no conflicts to declare.

Acknowledgements

References

1 A. L. Lehninger, D. L. Nelson, M. M. Cox and M. M. Cox, et al., Lehninger principles of biochemistry, Macmillan, 2005.
2 C. F. Bennett and E. E. Swayze, Annu. Rev. Pharmacol. Toxicol., 2010, 50, 259–293.
3 J. A. Doudna and E. Charpentier, Science, 2014, 346, 6213.
4 C. A. Batt, Science, 2007, 316, 1579–1580.
5 D. B. T. Cox, R. J. Platt and F. Zhang, Nat. Med., 2015, 21, 121–131.
6 A. V. Pinheiro, D. Han, W. M. Shih and H. Yan, Nat. Nanotechnol., 2011, 6, 763–772.
7 N. C. Seeman and H. F. Sleiman, Nat. Rev. Mater., 2017, 3, 1–23.

8 Y. Li, J. M. Artés, B. Demir, S. Gokce, H. M. Mohammad, M. Alangari, M. P. Anantram, E. E. Oren and J. Hihath, *Nat. Nanotechnol.*, 2018, **13**, 1167–1173.

9 J. Veselinovic, M. Alangari, Y. Li, Z. Matharu, J. M. Artés, E. Seker and J. Hihath, *Electrochim. Acta*, 2019, **313**, 116–121.

10 H. Miller, Z. Zhou, J. Shepherd, A. J. Wollman and M. C. Leake, *Rep. Prog. Phys.*, 2017, **81**, 024601.

11 Y. M. Sigal, R. Zhou and X. Zhuang, *Science*, 2018, **361**, 880–887.

12 K. G. G. P. Arachchillage, S. Chandra, A. Piso, T. Qattan and J. M. A. Vivancos, *J. Mater. Chem. B*, 2021, **9**(35), 6994–7006.

13 B. Xu, P. Zhang, X. Li and N. Tao, *Nano Lett.*, 2004, **4**, 1105–1108.

14 Y. Li, J. M. Artés and J. Hihath, *Small*, 2016, **12**, 432–437.

15 Y. Li, J. M. Artés, J. Qi, I. A. Morelan, P. Feldstein, M. P. Anantram and J. Hihath, *J. Phys. Chem. Lett.*, 2016, **7**, 1888–1894.

16 J. Hihath, B. Xu, P. Zhang and N. Tao, *Proc. Natl. Acad. Sci. U. S. A.*, 2005, **102**, 16979–16983.

17 J. M. Artés, Y. Li, J. Qi, M. Anantram and J. Hihath, *Nat. Commun.*, 2015, **6**, 1–8.

18 R. Zhuravel, H. Huang, G. Polycarpou, S. Polydorides, P. Motamarri, L. Katrivas, D. Rotem, J. Sperling, L. A. Zotti, A. B. Kotlyar, *et al.*, *Nat. Nanotechnol.*, 2020, **15**, 836–840.

19 L. Xiang, J. L. Palma, C. Bruot, V. Mujica, M. A. Ratner and N. Tao, *Nat. Chem.*, 2015, **7**, 221–226.

20 B. Xu and N. J. Tao, *Science*, 2003, **301**, 1221–1223.

21 J. Hihath and N. Tao, *Nanotechnology*, 2008, **19**, 265204.

22 L. Venkataraman, J. E. Klare, C. Nuckolls, M. S. Hybertsen and M. L. Steigerwald, *Nature*, 2006, **442**, 904–907.

23 H. Rascón-Ramos, J. M. Artés, Y. Li and J. Hihath, *Nat. Mater.*, 2015, **14**, 517–522.

24 R. I. Litvinov, O. Kononova, A. Zhmurov, K. A. Marx, V. Barsegov, D. Thirumalai and J. W. Weisel, *Proc. Natl. Acad. Sci. U. S. A.*, 2018, **115**, 8575–8580.

25 K. A. Minin, A. Zhmurov, K. A. Marx, P. K. Purohit and V. Barsegov, *J. Am. Chem. Soc.*, 2017, **139**, 16168–16177.

26 A. Zhmurov, O. Kononova, R. I. Litvinov, R. I. Dima, V. Barsegov and J. W. Weisel, *J. Am. Chem. Soc.*, 2012, **134**, 20396–20402.

27 Y. Matsunaga and Y. Sugita, *Curr. Opin. Struct. Biol.*, 2020, **61**, 153–159.

28 H. Geng, F. Chen, J. Ye and F. Jiang, *Comput. Struct. Biotechnol. J.*, 2019, **17**, 1162–1170.

29 A. Zhmurov, R. Dima, Y. Kholodov and V. Barsegov, *Proteins: Struct., Funct., Bioinf.*, 2010, **78**, 2984–2999.

30 M. J. Boniecki, G. Lach, W. K. Dawson, K. Tomala, P. Lukasz, T. Soltysinski, K. M. Rother and J. M. Bujnicki, *Nucleic Acids Res.*, 2016, **44**, e63.

31 T.-S. Lee, D. S. Cerutti, D. Mermelstein, C. Lin, S. LeGrand, T. J. Giese, A. Roitberg, D. A. Case, R. C. Walker and D. M. York, *J. Chem. Inf. Model.*, 2018, **58**, 2043–2050.

32 A. Zhmurov, K. Rybnikov, Y. Kholodov and V. Barsegov, *J. Phys. Chem. B*, 2011, **115**, 5278–5288.

33 D. A. Case, K. Belfon, I. Ben-Shalom, S. R. Brozell, D. Cerutti, T. Cheatham, V. W. D. Cruzeiro, T. Darden, R. E. Duke, G. Giambasu, *et al.*, AMBER 2020, University of California, San Francisco, 2020.

34 M. Zgarbová, M. Otyepka, J. Sponer, A. Mladek, P. Banas, T. E. Cheatham III and P. Jurecka, *J. Chem. Theory Comput.*, 2011, **7**, 2886–2902.

35 A. Pérez, I. Marchán, D. Svozil, J. Sponer, T. E. Cheatham III, C. A. Laughton and M. Orozco, *Biophys. J.*, 2007, **92**, 3817–3829.

36 J. A. Maier, C. Martinez, K. Kasavajhala, L. Wickstrom, K. E. Hauser and C. Simmerling, *J. Chem. Theory Comput.*, 2015, **11**, 3696–3713.

37 W. L. Jorgensen, J. Chandrasekhar, J. D. Madura, R. W. Impey and M. L. Klein, *J. Chem. Phys.*, 1983, **79**, 926–935.

38 C. Bruot, L. Xiang, J. L. Palma and N. Tao, *ACS Nano*, 2015, **9**, 88–94.

39 J. Sponer, G. Bussi, M. Krepl, P. Banas, S. Bottaro, R. A. Cunha, A. Gil-Ley, G. Pinamonti, S. Poblete, P. Jurecka, *et al.*, *Chem. Rev.*, 2018, **118**, 4177–4338.

40 I. Barbieri and T. Kouzarides, *Nat. Rev. Cancer*, 2020, **20**, 303–322.